Lasers in Surgery and Medicine 24:202–208 (1999)

Dynamic Modeling of Interstitial Laser Photocoagulation: Implications for Lesion Formation in Liver In Vivo

William Mark Whelan, PhD[1]* and Douglas Robert Wyman, PhD[2]

[1]Ryerson Polytechnic University, Toronto, Ontario, Canada
[2]McMaster University and Hamilton Regional Cancer Centre, Hamilton, Ontario, Canada

Background and Objective: **Interstitial Laser Photocoagulation (ILP) is a minimally invasive cancer treatment technique, whereby optical energy from implanted optical fibers is used to therapeutically heat small, solid tumors. In this work, the potential of ILP without tissue charring is investigated.**
Study Design/Materials and Methods: **Optical diffusion and bioheat transfer equations were used to develop dynamic models of interstitial laser heating in liver in vivo. Modifications in the optical properties due to tissue coagulation ($T \geqslant 60°C$) were incorporated into the physical description. In addition, the effect of three different blood perfusion patterns on temperature distributions was explored. Model-predicted temperatures were used as an index for thermal damage based on an accumulated temperature injury (Arrhenius) model. Thermal damage dimensions were determined with tissue temperatures constrained to remain below 100°C, so as to minimize the potential for tissue charring and smoke production.**
Results: **The model predicts that increases in scattering due to coagulation and choice of perfusion pattern affect substantially thermal damage dimensions. The results indicate that, for single fiber ILP at 2.55 W for 600 s, the maximum achievable thermal damage diameter in liver, without charring, is 9.6 mm. In addition, ILP performed with high-low power ramping may have an advantage over constant power treatments, in that, larger volumes of thermal damage can be realized earlier in an irradiation.**
Conclusions: **For ILP performed with a single spherical emitting fiber, optimal irradiation parameters exist such that thermal lesions in liver up to approximately 10 mm in diameter can be induced while the maximum tissue temperature remains below 100°C, avoiding tissue charring. Lasers Surg. Med. 24:202–208, 1999.** **© 1999 Wiley-Liss, Inc.**

Key words: charring; coagulation; optimization; optothermal modeling; perfusion

INTRODUCTION

Small unresectable tumors can be destroyed thermally using interstitial laser photocoagulation [1,2]. This minimally invasive technique involves coupling continuous-wave laser energy to optical fibers implanted in a tumor volume. At temperatures above 60°C, tissue proteins denature resulting in thermal coagulative necrosis [3]. After irradiation, the small volume of damaged tissue is absorbed or isolated by the body. Clinically, ILP has been used to destroy small unresectable tumors in many organs including breast [4], brain [5] and liver [1]. Frequently, tissue tem-

*Correspondence to: Dr. William M. Whelan, Department of Mathematics, Physics and Computer Science, Ryerson Polytechnic University, 350 Victoria Street, Toronto, Ontario M5B 2K3, Canada.

Accepted 3 September 1998

peratures near the fiber-tip surpass 100°C, resulting in vaporization of tissue water. Tissue charring follows quickly after vaporization and is concomitant with smoke production (includes CO)[3]. Although the significance of intravascular gas production remains unclear, it is generally accepted that it should be avoided, because of the potential for air emboli in the circulatory system. Investigations to minimize the potential for charring have utilized fluid irrigation to cool tissues [6] and diffusing fiber tips [7,8] to reduce optical power densities. However, charring appears to have the advantage of producing larger lesions [9]. The potential of ILP without tissue charring has yet to be thoroughly investigated.

A theoretical investigation of lesion formation in liver, during single fiber ILP at 1,064 nm irradiation, is presented for the case when the maximum tissue temperature remains below 100°C, which avoids vaporization, charring, and smoke production. The influence on thermal damage dimensions of blood perfusion pattern and coagulation-induced increased scattering is investigated. Thermal damage is assessed using an accumulated temperature injury (Arrhenius) model.

THEORY

Optical propagation and heat transfer are modeled using diffusion theory and the Pennes bioheat transfer equation, respectively, given by

$$-\nabla\cdot D\,\nabla\phi + \mu_a\phi = S \qquad (1)$$

$$\rho_t c_t \frac{\partial T}{\partial t} = \nabla\cdot k_t \nabla T - w_b' c_b (T - T_a) + Q_L \qquad (2)$$

where D (cm) is the diffusion coefficient ($D = [3(\mu_a + \mu_s')]^{-1}$), μ_a (cm^{-1}) is the optical absorption coefficient, μ_s' (cm^{-1}) is the optical reduced scattering coefficient, ϕ (W/cm^2) is the optical fluence rate, ρ_t (g/cm^3) is the tissue density, c_t (J/g/°C) is the tissue heat capacity, k_t (W/cm/°C) is the tissue thermal conductivity, w_b' ($g/cm^3/s$) is the average volumetric blood perfusion rate, c_b is the blood heat capacity, and T and T_a are the tissue and arterial blood temperatures, respectively. The blood perfusion rate, w_b (ml/100 g/min), generally found in the literature is related to (2) by $w_b' = 100(w_b\ \rho_t\ \rho_b)$, where ρ_b (g/cm^3) is the blood density. For deposition of optical energy, $Q_L = \mu_a\ \phi$. Note that Q_L is the term that links the mathematical descriptions of optical propagation (1) and heat transfer (2).

The coupled equations (1) and (2) were solved for $\phi(r)$ and T(r,t), respectively, using a central finite difference scheme for a sphere of radius 30 mm, with 0.1 mm node spacing and a 5 s temporal step. The model was also insensitive to increment changes near these values. The light source (i.e., optical fiber tip) is located at r = 0, the center of the spherical tissue volume.

Complete thermal damage is assessed based on the time-temperature history of tissues, as described by Arrhenius theory and used by many other authors [10–12]. Predicting the accumulation of thermal injury using time-temperature data involves evaluating an Arrhenius damage integral at multiple locations in the treatment field. This approach can be computationally intensive. In this work, an approximation to the Arrhenius damage integral is used. With this approximation, the extent of tissue damage is described in terms of an equivalent time exposure at 43°C, t_{43}, given by [13]

$$t_{43} = \sum_{t=t_o}^{t=t_{\text{final}}} C_o(T)^{(43-T_{\text{avg}})}\,\Delta t \qquad (3)$$

where T_{avg} is the time-average temperature during the time interval, Δt. Experimental Arrhenius plots of time-temperature data to produce an isoeffect in a variety of tissues indicate that C_o (T) = 0.5 for T > 43°C and C_o (T) = 0.25 for T < 43°C [13]. In other words, the time required to reach an isoeffect is decreased two-fold for each degree rise in temperature above 43°C and is increased four-fold for each degree fall below 43°C. The threshold value of t_{43} depends on tissue-type. Experimental evidence for protracted exposures at hyperthermic temperatures indicates that exposing tissues to 43°C for 1 hour (t_{43} = 3,600 s) induces necrosis in a variety of tissue-types [13].

Equation (3) may not be a good predictor of thermal damage at high temperatures such as induced during ILP. However, observations of thermal damage in canine bladder in vivo [14] at temperatures up to 60°C are consistent with accumulated temperature injury models. Furthermore, an injury model [15] similar to (3), but with C_o (T) = 0.5 for T ⩾ 44°C, predicted reasonably the dimensions of laser-induced thermal necrosis in canine liver [16].

Therefore, in this work, thermal damage was predicted using (3). The accumulated value of t_{43}, at each finite difference grid point in the thermal field, was computed at each time step during for-

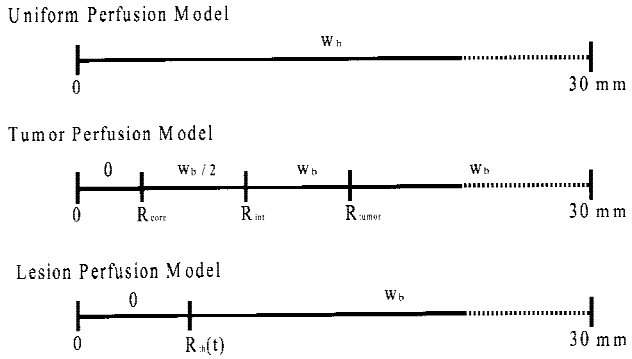

Fig. 1. Static and dynamic approximations for blood perfusion patterns in tissue during ILP. $R_{th}(t)$, determined by (3), increases from an initial value of zero during the irradiation.

ward calculations. At grid points where $t_{43} \geqslant 3{,}600$, the model predicted thermal damage to have occurred. The thermal damage radius, $R_{th}(t)$, was determined by the radial location where the accumulated value $t_{43} = 3{,}600$. $R_{th}(t)$ was updated at each time step during forward calculations.

In many instances, published models of ILP have assumed temporally invariant optical properties and blood perfusion patterns. This assumption is poor, because coagulation has been shown to increase optical scattering [12, 17], and blood perfusion in necrotic and viable tissues would most certainly differ. In this work, a 60°C coagulation threshold model was used, which assumes that coagulation occurs instantaneously in tissues exposed to a temperature of 60°C. Coagulation-induced increased optical scattering was modeled as a step increase in μ_s' extending from the source to the 60°C isotherm, defined as the coagulation radius $R_{coag}(t)$.

Three blood perfusion patterns, shown in Figure 1, were investigated based on a published mean perfusion rate in liver of $w_b = 100$ ml/100 g/min [18]. In the uniform perfusion model, a constant perfusion rate for $r > 0$ was considered. In the three-zone tumor perfusion model, a 10 mm diameter spherical tumor ($R_{tumor} = 5$ mm) was considered and characterized by regions of no perfusion ($r < R_{core}$), intermediate perfusion ($R_{core} < r < R_{int}$) and maximum perfusion ($r > R_{int}$), with $R_{core} = 1$ mm, $R_{int} = 3$ mm. In the lesion perfusion model, a radially expanding zone of non-perfused necrotic tissue bounded by R_{th} (t) was considered.

An ambient tissue temperature of 37°C was used in all simulations. Values for $R_{coag}(t)$ and $R_{th}(t)$ were updated every 5 s during forward calculations. Single fiber ILP at 1064 nm in normal liver was simulated by using the published values for the optical and thermophysical properties and blood perfusion rates shown in Table 1.

RESULTS AND DISCUSSION

Given the range of experimentally measured coagulation-induced increases in scattering reported in the literature [12, 17], a parametric assessment was undertaken in which the reduced scattering coefficient for coagulated liver, $(\mu_s')_{coag}$, is approximated as either a 2-, 4-, or 6-fold increase over that for normal liver, $(\mu_s')_{norm}$.

The calculated thermal history at a radial distance of 1 mm from the source, for a 600 s irradiation of 3 W, is shown in Figure 2a. A uniform perfusion rate of 100 ml/100 g/min was used in calculating temperatures. Transient temperature profiles are identical prior to the predicted time of onset of coagulation, ~ 70 s. At $t > 70$ s, the temperature increase with increasing $(\mu_s')_{coag}$ is nonlinear. However, the thermal histories for a constant and a twofold increase in the reduced scattering coefficient are similar, indicating that temperature differences are limited to within 1 mm of the optical fiber. Thermal equilibrium is reached early in the irradiation, ~ 100 s for the homogeneous case $(\mu_s')_{coag} = (\mu_s')_{norm}$, and is delayed with increasing $(\mu_s')_{coag}$.

The predicted coagulation diameter as a function of time and $(\mu_s')_{coag}$, is shown in Figure 2b. The observed step-like increases in coagulation diameter is a result of discretization in the finite difference technique, such that R_{coag} (t) increases in 0.1 mm increments. Prior to the onset of coagulation, R_{coag} (t) is zero. At 70 s the model-predicted temperature at the first radial node, $r = 0.1$ mm, has exceeded 60°C. For $t > 70$ s, the time rate of increase in the coagulation diameter depends greatly on the value of $(\mu_s')_{coag}$. At 600 s, the model-predicted coagulation diameter is 0.95 mm, 1.15 mm, 2.15 mm, and 3.95 mm for $(\mu_s')_{coag}/(\mu_s')_{norm}$ of 1, 2, 4, and 6, respectively.

The observed non-linear relationship between model-predicted coagulation diameters and increased $(\mu_s')_{coag}$ is expected given the similar relationship between fluence rate and μ_s' in (1). For $t > 70$ s, the maximum fluence rate near the source, inside the expanding coagulation radius, increases with increasing $(\mu_s')_{coag}$, thereby increasing the maximum energy deposition rate, $Q_L = \mu_a \phi(r)$. This induces higher temperatures near the source and, in turn, further broadens the co-

TABLE 1. Thermophysical and Blood Perfusion Properties [18] and Optical Properties [19] Used in the Calculational Model

Tissue thermal conductivity (human liver)	0.00520 W/cm/°C
Specific heat of tissue (human liver)	3.60 J/g/°C
Tissue density (human liver)	1.06 g/cm^3
Blood perfusion rate (human liver)	100 ± 80 ml/100 g/min
Specific heat of blood	3.84 J/g/°C
Blood density	1.06 g/cm^3
Absorption coefficient (bovine liver)	0.53 cm^{-1}
Reduced scattering coefficient (bovine liver)	1.76 cm^{-1}

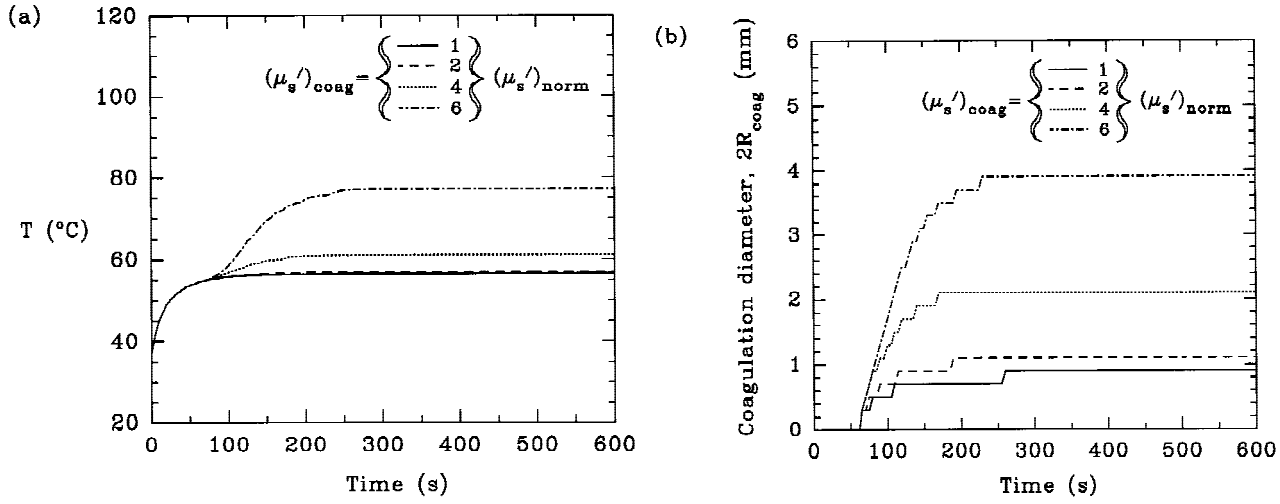

Fig. 2. Effect of coagulation-induced increases in the reduced scattering coefficient on the model predicted (**a**) thermal history at 1 mm from the source and (**b**) coagulation diameters in liver for a 600 s irradiation at 3 W. A uniform perfusion rate of w_b = 100 ml/100 g/min was used in calculating these results.

agulation zone, as observed in Figure 2b. Since all photons emitted by the source are absorbed somewhere, the spatial integral of $\mu_a\phi(r)$ must be equal to 3 W for all $(\mu_s')_{coag}$ modeled. Therefore an increase in the fluence rate near the source is accompanied by a decrease away from the source.

Figure 2 indicates that, in the absence of vaporization and charring, coagulation-induced increases in scattering in liver affect temperatures substantially and should be considered when modeling ILP. However if temperatures exceed 100°C, vaporization and charring are likely to occur and tissue temperatures are much less influenced by optical scattering.

Uniform blood perfusion has been shown to reduce radial temperature profiles during laser heating [20]. However, uniform perfusion is a rough approximation of real tissue behavior. The effect of three different blood perfusion patterns (see Fig. 1) on thermal damage dimensions for a 600 s irradiation at 2.5 W is shown in Figure 3. A scattering increase of $(\mu_s')_{coag} = 4(\mu_s')_{norm}$ was used. Again, $R_{th}(t)$ increases in 0.1 mm incre-

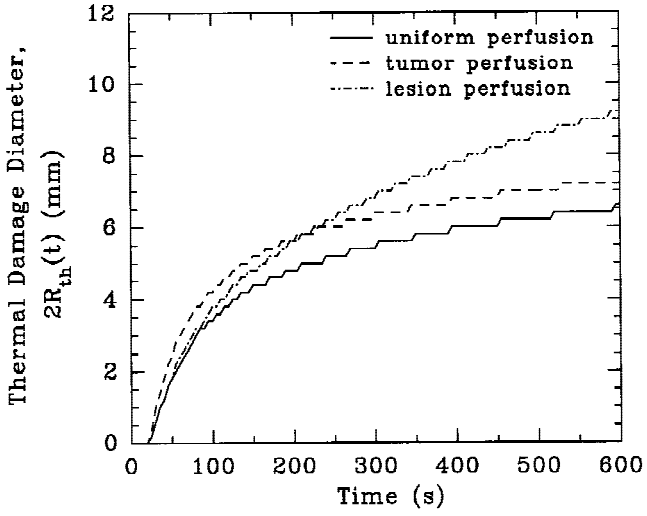

Fig. 3. Effect of perfusion pattern on model-predicted thermal damage diameter in liver during a 600 s irradiation at 2.5 W. Perfusion patterns shown in Figure 1, with w_b = 100 ml/100 g/ min, were used to calculate temperatures.

ments based on the finite difference scheme. The model-predicted damage dimensions shown in Figure 3 are markedly different. Thermal damage predicted with tumor perfusion always exceeds that with uniform perfusion. This is expected given that the tumor perfusion model assumes no blood flow within 1 mm from the fiber tip, resulting in appreciably higher temperatures at the fiber tip than those predicted using uniform perfusion. Figure 3 indicates that thermal damage based on a lesion perfusion model will continue to expand at longer irradiation times as $R_{th}(t)$ continues to increase due to accumulated low temperature injury. Therefore thermal equilibrium can only be approximated. The diameters of thermal damage predicted by the tumor and lesion perfusion approximations cross at 6 mm, corresponding to the static 3 mm intermediate perfusion radius, R_{int}, assumed in the tumor perfusion model. If $R_{th}(t)$ in the lesion perfusion approximation is greater than R_{int} in the tumor perfusion approximation, the former will predict greater thermal damage.

Maximizing tissue damage while maintaining temperatures below 100°C is a laser power and exposure optimization problem. In addition, the blood perfusion rate in liver is highly variable (20–180 ml/100 g/min). The model was used to determine the laser power required to induce a maximum tissue temperature just below 100°C in liver as a function of perfusion rate for a 600 s irradiation. The lesion perfusion approximation with $(\mu_s')_{coag} = 4(\mu_s')_{norm}$ was used. The coagulation and thermal damage dimensions induced at maximal power are shown in Figure 4. As expected, the predicted thermal damage diameters are larger than the coagulation diameters, given that the former includes accumulated low temperature injury. The model-predicted temperature at the boundary of thermal damage, for each perfusion rate investigated, is 47.7°C. It is observed in Figure 4 that as the perfusion rate increases, the power can be increased while still maintaining a maximum tissue temperature just below 100°C. However, coagulation and thermal damage dimensions are reduced.

The results in Figure 4 suggest that pretreatment calculations may prove useful only in cases where the perfusion rate is known. Figure 4 indicates that for an average blood perfusion rate of 100 ml/100 g/min, single fiber ILP for 600 s can produce maximum coagulation and thermal damage diameters of 5.6 mm and 9.6 mm, respectively, without charring. This was achieved for a

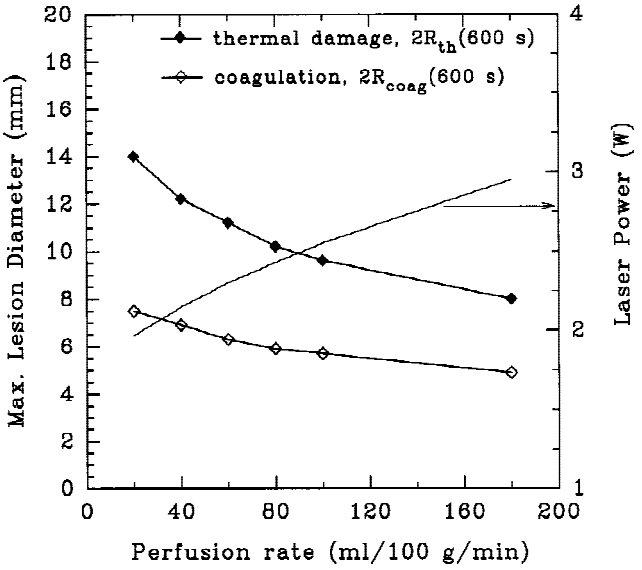

Fig. 4. Model-predicted maximum thermal damage and coagulation diameters for a 600 s irradiation in liver as a function of perfusion rate. For each perfusion rate, the laser power required to induce a maximum tissue temperature just below 100°C is plotted (refer to the right vertical axis). The lesion perfusion approximation was used to calculate temperatures.

continuous laser power of 2.55 W, such that the maximum tissue temperature remained just below 100°C. These results indicate that, using a single plane-cut optical fiber, vaporization and possibly carbonization is required to produce in vivo lesions in liver greater than ~ 10 mm, consistent with experimental evidence [7]. This suggests that multiple source fiber arrangements may be required to induce, without charring, liver lesions larger than 10 mm in diameter.

Frequently, ILP is performed using constant laser power such that tissue temperatures are maximum near the end of the irradiation. The mathematical model was used to investigate temperature profiles and thermal damage dimensions in liver in vivo ($w_b = 100$ ml/100 g/min) for a 600 s irradiation at 1,064 nm based on two laser power deposition schemes: 1) a constant power of 2.55 W ($t > 0$) and 2) a power ramp-down of 5.0 W ($t < 30$ s), 3.0 W ($30 \leq t \leq 60$ s), and 2.5 W ($t > 60$ s). Laser power values were optimized to ensure that the maximum tissue temperatures for both schemes were similar and that tissue charring was avoided. The maximum tissue temperature histories for the two laser power schemes are shown in Figure 5a. It is observed in Figure 5a that, for ramp-down power, there is a substantial increase in heating early in the irradiation compared to constant power.

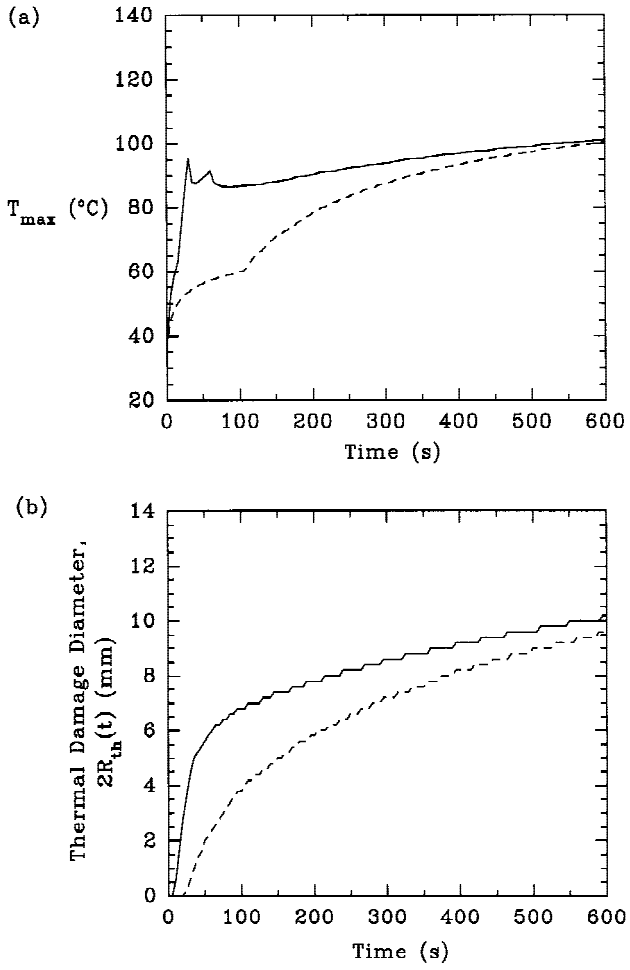

Fig. 5. (**a**) Maximum tissue temperature histories, at r = 0.1 mm, in liver and the (**b**) corresponding thermal damage diameter produced for constant power (----) and high-low power ramping (—) schemes. The lesion perfusion approximation (w_b = 100 ml/100g/min) and $(\mu_s')_{coag} = 4(\mu_s')_{norm}$ were used to calculate temperatures.

Thermal damage formation for the two power schemes is shown in Figure 5b. Final damage diameters at 600 s differ by only 0.5 mm. However, Figure 5b indicates that greater thermal damage can be realized earlier in the irradiation using a high-low power ramp-down scheme. Compare 375 s required to induce a 8 mm diameter lesion, based on constant power, to 210 s required to induce the same lesion utilizing the ramp-down power scheme. This may be important in clinical settings where there is a potential for optical fibers and temperature sensors to be displaced during treatment. Interestingly, the predicted thermal damage diameters, for a fixed energy deposition of 1,000 J, are 8.0 mm and 9.0 mm for the constant and ramp-down power schemes, respectively. This suggests that a ramp-down power scheme may induce greater thermal damage compared to a constant power scheme, for the same total energy deposition.

The results presented do not consider modifications in μ_a due to the presence of blood. The absorption coefficient for hemoglobin in the near infrared is approximately five times that of normal bovine liver ex vivo [19], suggesting that any modeled increase in optical absorption would likely quicken the predicted onset of water vaporization and charring. However, the optical properties of in vivo tissues are not well determined and, therefore, quantifying the increase in optical absorption has yet to be realized. Furthermore, blood perfusion in tissues is highly variable and any increase in optical absorption would most certainly be coupled with the perfusion rate.

The temperature dependence of optical properties in vivo is also not well known. Jaywant et al. [21] reported a near-linear increase in μ_s' with temperature from 30 to 70°C in bovine muscle ex vivo at 810 nm. Therefore, the instantaneous step increase in μ_s', used in our model, likely underestimates changes in μ_s' in tissues exposed to temperatures below 60°C and overestimates these changes in tissues exposed to temperatures above 60°C. However, Prapavat et al. [22] modeled coagulation-increased scattering based on a 60°C threshold description and reported reasonable agreement between model-predicted and experimentally measured lesions.

The 60°C threshold coagulation model seems to be a good predictor of coagulation dimensions at early and intermediate times. However, tissue coagulation has been observed to increase long after thermal equilibrium has been established [23], indicating that an Arrhenius coagulation model would be a better predictor of coagulation dimensions near steady state. This work provides a basis with which to conduct experimental studies ex vivo and in vivo in order to further evaluate optimal irradiation parameters for maximum damage without charring.

CONCLUSIONS

This theoretical study has focused on investigating the potential of ILP in liver without tissue charring. It is evident that the modeling of thermal processes requires accurate knowledge of the optical properties and blood perfusion patterns, both of which can be spatially and temporally dependent. However, dynamic changes in tissue properties during treatment are not well

known. The mathematical model presented provides a tool for identifying trends in lesion formation in liver as a function of irradiation parameters and blood perfusion pattern. The results demonstrate that coagulation-induced increases in scattering and choice of perfusion pattern affect substantially model predictions of coagulation and thermal damage dimensions. Models of ILP based on uniform optical scattering and perfusion will certainly underestimate temperatures near the optical fiber tip. The results indicate that optimal irradiation parameters exist such that clinically relevant tissue volumes can be treated, while the maximum tissue temperature remains below 100°C, which avoids tissue charring. For a single spherical emitting fiber, 8–10 mm diameter lesions in liver may be achievable without tissue charring. In addition, ILP performed with high-low power ramping may have an advantage over constant power applications, in that, larger volumes of thermal damage can be realized earlier in an irradiation. However, given the limited knowledge of tissue blood perfusion, optimal laser power ramping will likely require a feedback mechanism, such as temperature or image feedback, in order to maximize damage while preventing tissue temperatures at the fiber tip from exceeding 100°C.

REFERENCES

1. Amin Z, Bown SG, Lees WR. Liver tumor ablation by interstitial laser photocoagulation: review of experimental and clinical studies. Sem Interven Rad 1993; 10:88–100.
2. Wyman DR, Schatz SW, Maguire JAC. Comparison of 810 nm and 1064 nm wavelengths for interstitial laser photocoagulation in rabbit brain. Lasers Surg Med 1997; 21:50–58.
3. Thomsen S. Pathologic analysis of photothermal and photomechanical effects of laser-tissue interactions. Photochem Photobiol 1991; 53:825–835.
4. Harries SA, Amin Z, Smith MEF, Lees WR, Cooke J, Cook MG, Scurr JH, Kissin MW, Bown SG. Interstitial laser photocoagulation as a treatment for breast cancer. Br J Surg 1994; 81:1617–1619.
5. Roux FX, Merienne L, Leriche B, Lucerna S, Turak B, Devaux B, Chodkiewicz JP. Laser interstitial thermotherapy in stereotactical neurosurgery. Laser Med Sci 1992; 7:121–126.
6. Anvari B, Motamedi M, Torres JH, Rastegar S, Orihuela E. Effects of surface irrigation on the thermal response of tissue during laser irradiation. Lasers Surg Med 1994; 14:386–395.
7. van Hillegersberg R, van Staveren HJ, Kort WJ, Zondervan PE, Terpstra OT. Interstitial Nd:YAG laser coagulation with a cylindrical diffusing fiber tip in experimental liver metastases. Lasers Surg Med 1994; 14:124–138.
8. Orth K, Russ D, Duerr J, Hibst R, Steiner R, Beger HG. Thermo-controlled device for inducing deep coagulation in the liver with the Nd:YAG laser. Lasers Surg Med 1997; 20:149–156.
9. Amin Z, Buonaccorsi G, Mills T, Harries S, Lees WR, Bown SG. Interstitial laser photocoagulation: evaluation of a 1320 nm Nd-YAG and an 805 nm Diode Laser: the significance of charring and the value of precharring the fibre tip. Laser Med Sci 1993; 8:113–120.
10. Beacco CM, Mordon SR, Brunetaud JM. Development and experimental in vivo validation of mathematical modeling of laser coagulation. Lasers Surg Med 1994; 14:362–373.
11. Glenn TN, Rastegar, S, Jacques SL. Finite element analysis of temperature controlled coagulation in laser irradiated tissue. IEEE Trans Biomed Eng 1996; 43:79–86.
12. Agah R, Gandjbakhche AH, Motademi M, Nossal R, Bonner RF. Dynamics of temperature dependent optical properties of tissue: dependence on thermally induced alteration. IEEE Trans Biomed Eng 1996; 43:839–846.
13. Sapareto SA, Dewey WC. Thermal dose determination in cancer therapy. Int J Rad Oncol Biol Phys 1984; 10:787–800.
14. Linke C, Elbadawi A, Netto V, Roberts A, Russo M. Effect of marked hyperthermia upon canine bladder. J Urology 4 1972; 117:599–602.
15. Davies M, Dowden J, Steger A, Kapadia P, Whiting P. A mathematical model for interstitial laser treatment of tumors using four fibers. Laser Med Sci 1989; 4:41–53.
16. Steger AC, Bown SG, Clark CG. Interstitial laser hyperthermia-studies in normal liver. Br J Surg 1988; 75:598.
17. Splinter R, Svenson RH, Littmann L, Tuntelder JR, Chuang CH, Tatsis GP, Thompson M. Optical properties of normal, diseased and laser photocoagulated myocardium at the Nd:YAG wavelength. Lasers Surg Med 1991; 11:117–124.
18. Duck FA. Physical Properties of Tissue. London: Academic Press, 1990.
19. Cheong WF, Prahl SA, Welch AJ. A review of the optical properties of biological tissues. IEEE J Quantum Electron 1990; 26:2166–2185.
20. Anvari B, Rastegar S, Motamedi M. Modeling of intraluminal heating of biological tissue: implications for treatment of benign prostatic hyperplasia. IEEE Trans Biomed Eng 1994; 41:854–864.
21. Jaywant S, Wilson B, Patterson M, Lilge L, Flotte T, Woolsey J, McCulloch C. Temperature dependent changes in the optical absorption and scattering spectra of tissues. SPIE Proc 1993; 1882: 218–229.
22. Prapavat V, Roggan A, Walter J, Beuthan J, Klingbeil U, Muller G. In vitro studies and computer simulations to assess the use of a diode laser (850 nm) for laser-induced thermotherapy (LITT). Lasers Surg Med 1996; 18:22–33.
23. Wyman D, Wilson B, Adams K. Dependence of laser photocoagulation on interstitial delivery parameters. Lasers Surg Med 1994; 14:59–64.